

Moments of the Proton F_2 Structure Function at Low Q^2

C.S. Armstrong,¹ R. Ent,¹ C.E. Keppel,^{1,2} S. Liuti,^{3,4} G. Niculescu,^{1,5} I. Niculescu^{1,6}

¹ Thomas Jefferson National Accelerator Facility. ² Hampton University. ³ University of Virginia. ⁴ INFN Sezione di Roma Tre. ⁵ Ohio University. ⁶ George Washington University.

(May 25, 2000)

We review the status of inclusive electron-proton scattering F_2 structure function data in both the nucleon resonance region and the deep inelastic region, at momentum transfers below 5 (GeV/c)². From these data we construct moments of F_2 , down to momentum transfers of $Q^2 \approx 0.1$ (GeV/c)². The second moment is only slowly varying with Q^2 down to $Q^2 \approx 1$, which is a reflection of duality. Below Q^2 of 1 (GeV/c)², the Q^2 dependence of the moments is predominantly governed by the elastic contribution, whereas the inelastic channels still seem governed by local duality.

I. INTRODUCTION

Three decades ago, Bloom and Gilman observed a fascinating correspondence between the resonance electroproduction and deep inelastic kinematic regimes of inclusive electron-nucleon scattering [1,2]. Specifically, it was observed that the resonance strength could be related to the deep inelastic strength via a scaling variable which allowed the comparison of the lower missing mass squared, W^2 , and lower four-momentum squared, Q^2 , resonance region data to the higher W^2 and Q^2 deep inelastic data. It was observed that the deep inelastic data are apparently equivalent to an average of the resonance region data. Further, this behavior was observed over a range in Q^2 and W^2 , and it was found that, with changing Q^2 , the resonances move along, but always average to, the smooth scaling curve typically associated with deep inelastic scattering. This behavior clearly hinted at a common origin for resonance (hadron) electroproduction and deep inelastic (partonic) scattering, termed parton-hadron, or Bloom-Gilman, duality.

A global kind of parton-hadron duality is well established: low-energy resonance production can be shown to be related to the high-energy behavior of hadron-hadron scattering [3]; the familiar ratio of $e^+e^- \rightarrow$ hadrons over $e^+e^- \rightarrow$ muons uses duality to relate the hadron production to the sum of the squared charges of the quarks: here duality is guaranteed by unitarity (in this, one could argue that the ρ production channel exhibits local duality, in that it's area averages to about the same global value) [4]; in Perturbative QCD (PQCD) the high-momentum transfer behavior of nucleon resonances can be related to the high-energy transfer behavior of deep inelastic scat-

tering [4,5]. However, it is not clear why duality should also work in a localized region, and even at relatively low momentum transfers.

Inclusive deep inelastic scattering on nucleons is a firmly-established tool for the investigation of the quark-parton model. At large enough values of invariant mass squared W^2 ($= M^2 + Q^2(1/x - 1)$, with M the proton mass and x the Bjorken scaling variable) and four-momentum transfer squared Q^2 , QCD provides a rigorous description of the physics that generates the Q^2 behavior of the nucleon structure function $F_2 = \nu W_2$. The well-known logarithmic scaling violations in the F_2 structure function of the nucleon, predicted by asymptotic freedom, played a crucial role in establishing QCD as the accepted theory of strong interactions [6,7]. Such behavior becomes especially transparent in comparing high Q^2 (≥ 10 (GeV/c)²) Cornwall-Norton or Nachtmann moments [8] of F_2 structure functions with the logarithmic formulae of asymptotic freedom [5,9].

An analysis of the resonance region at smaller W^2 and Q^2 in terms of QCD was first presented in Refs. [10,11], where Bloom and Gilman's duality was re-interpreted, and the integrals of the average scaling curves were equated to the $n=2$ moment of the F_2 structure function. The Q^2 dependence of these moments can be described by ordering the contributing matrix elements according to their twist (= dimension - spin) in powers of $1/Q^2$. It was concluded [10] that the fall of the resonances along a smooth scaling curve with increasing Q^2 was attributed [10] to the fact that there exist only small changes in these lower moments of the F_2 structure function due to higher twist effects. These higher twist effects can be regarded as interactions between the quark struck in the electron-nucleon scattering process and the other quarks in the nucleon. Such effects are inversely proportional to Q^2 , and can therefore be large at small Q^2 . If they are not, averages of the F_2 structure function over a sufficient range in x at moderate and high Q^2 are approximately the same. Notwithstanding, the dynamical origin of local duality, and thus the reason why the higher-twist contributions, undoubtedly required to construct the coherent nucleon resonances, tend to largely cancel on average, even at momentum transfers below 5 (GeV/c)², is still not understood [9,12].

Recently, it was surprisingly found that the resonance region seems to average around a global scaling curve down to very low values of the four-momentum transfer squared, $Q^2 \approx 0.2$ (GeV/c)². This global scaling curve

mimics a behavior as could be expected if one *solely* deals with valence-like quarks [13]. Due to the large increase in high-precision electron-proton scattering data over the last twenty years, we revisit the F_2 structure function moment analysis, with the aim to shed light on why local duality works at far smaller Q^2 than anticipated, and why the nucleon resonance spectra tend to average to a scaling curve mimicking a valence-like quark distribution. For this, we present here a moment analysis in a Q^2 range of 0.1 - 5 (GeV/c)².

II. LOCAL DUALITY AT LOW MOMENTUM TRANSFER

First, we show in Fig. 1 an overview of recent high-precision proton resonance F_2 data at low Q^2 [14]. We also include data from SLAC at $Q^2 < 0.3$ (GeV/c)² [15]. For the former, the systematic uncertainty is estimated to be 3.5% [14]. For the latter, due to uncertainties in absolute normalization and radiative corrections, we estimate the systematic uncertainty to be better than 10%. The solid curves represent, for the different kinematics, the single scaling curve defined by averaging *all* nucleon resonance F_2 data, regardless of Q^2, W^2 , as a function of Nachtmann ξ ($= 2x/(1 + \sqrt{1 + 4M^2x^2/Q^2})$ [8]). We have constrained the scaling curve, relevant for the large ξ region, to a model of higher Q^2 SLAC data [16]. The resulting parameterization of this scaling curve is [14]

$$F_2 = \xi^{0.870}(1 - \xi)^{0.006} [0.005 - 0.058(1 - \xi) - 0.017(1 - \xi)^2 + 2.469(1 - \xi)^3 - 0.240(1 - \xi)^4]. \quad (1)$$

As one can see from Fig. 1, the individual spectra, at various Q^2 , oscillate around this single-curve parameterization. We emphasize that this is *not* by construction, as the parameterization, at any given value of ξ , is obtained from a range of nucleon resonance data at variant values of Q^2 and W^2 (e.g., the second resonance bump could have always been below the scaling curve, while the first above, etc.). Apparently, nature forces the oscillatory behavior of the various resonance bumps around this scaling curve, which, at $\xi > 0.3$, corresponding to $Q^2 \geq 1$ (GeV/c)² in the nucleon resonance region, closely resembles the F_2 deep inelastic scattering behavior [14], and for $\xi < 0.3$, corresponding to $Q^2 \leq 0.5$ (GeV/c)² in the nucleon resonance region, mimics [13] xF_3 data obtained from averaging neutrino and antineutrino deep inelastic scattering data [17]. The latter, to leading order in QCD, selects the difference of quark and antiquark distribution functions, is predominantly sensitive to a valence quark only distribution.

Increasing from $Q^2 \approx 0.07$ (GeV/c)² (Fig. 1a) to $Q^2 \approx 3$ (GeV/c)² (Figs. 1h,1i) the F_2 spectra change shape drastically. The low Q^2 spectrum shows a predominant $N - \Delta$ transition (we do not show the elastic peak, huge

at this Q^2), and relatively minor strength at larger energy transfers. This is not surprising, at these relatively small energy and four-momentum transfers one would expect to predominantly excite the valence quarks. At $Q^2 = 3.0$ (GeV/c)², on the other hand, one sees that the nucleon resonances are largely reduced, and the inelastic background enhanced. Furthermore, F_2 in the higher resonance regions is larger than F_2 in the $N - \Delta$ transition region. Apparently, a swap of strength has occurred between the various channels.

To further illustrate how the nucleon resonances seem to follow a valence-like curve, we show in Fig. 2 the behavior of the $N - \Delta$ transition region (here defined as $1.2 < W^2 < 1.9$ GeV²) and the second resonance region (defined as $1.9 < W^2 < 2.5$ GeV²) for various Q^2 as a function of ξ , in comparison with the global scaling curve defined above. As concluded in Refs. [13,14], it seems that the nucleon resonances slide along one global scaling curve (note that the difference between Figs. 1 and 2 is in essence just the conversion from W^2 to ξ , for fixed Q^2). One can see that, if nature forces the oscillatory behavior around a global scaling curve at low Q^2 , the resonance excitation strengths will necessarily grow if they are in the region below the $\xi \approx 0.25$ where the maximum of the global scaling curve occurs, and subsequently decrease once the maximum of the global scaling curve has been crossed. Compare for instance the behavior of the $N - \Delta$ transition with the larger-mass resonance regions: at $Q^2 = 0.45$ (GeV/c)² (solid circles in Fig. 2 (top), and Fig. 1c) the $N - \Delta$ transition strength is large being at about the maximum of the scaling curve. Its strength, as for all $Q^2 < 0.45$ (GeV/c)², is also larger than the higher-mass resonances which lie at lower ξ for the same Q^2 . On the other hand, for $Q^2 \approx 3.0$ (GeV/c)² (open circles in Fig. 2(top), and Fig. 1h) the $N - \Delta$ transition strength is small because it is positioned at large ξ , and smaller than the higher-mass resonances that lie at lower values of ξ , but have crossed the maximum of the scaling curve. The smooth curve, to which the nucleon resonances tend, determines the momentum transfer dependence of the various nucleon resonance regions, forcing the nucleon elastic and transition form factors to scale like Q^{-4} [18] at relatively small Q^2 , and therefore resemble the Q^{-4} scaling as predicted by PQCD.

In Fig. 3 we show a compilation of the world's electron-proton scattering data for the F_2 structure function at low Q^2 . The deep inelastic (invariant mass squared $W^2 > 4$ GeV²) data originate from SLAC [19], CERN (NMC) [20], FNAL (E665) [21], and DESY (H1,ZEUS) [22-27]. As before we include data from the proton resonance region from SLAC [15] and JLab [13]. The solid curves indicate the next-to-leading order parameterizations of Glück, Reya, and Vogt (GRV) [28,29], which use input parton distributions starting from very low Q^2 values. In the third panel of Fig. 3, the GRV calculation is in fact the GRV input distribution at $Q^2 = 0.4$ (GeV/c)² [29],

without any evolution, *neglecting sea and gluon contributions*. As one can see the proton resonance region data for $Q^2 = 3.1$ (GeV/c)² and $Q^2 = 0.9$ (GeV/c)² smoothly join the deep inelastic data, and agree well with the GRV next-to-leading order calculations, exhibiting the local duality witnessed by Bloom and Gilman [1,2].

Turning our attention to the bottom two panels of Fig. 3, the low Q^2 F_2 data, we are only left with the recent DESY data [25,26], some sparse FNAL data [21], and the nucleon resonance data [15,13]. The DESY data exhibit the well-known collapse of the proton structure functions at (very) small x . One interpretation of this effect is that, at these small Q^2 , one sees a smooth transition from deep inelastic scattering to the real photon point at $Q^2 = 0$ [26,30,27]: gauge invariance requires that for consistency near $Q^2 = 0$ the structure function F_2 for inelastic channels must vanish like $Q^2\sigma(\gamma p)/(4\pi^2\alpha_{em})$ [30]. On the other hand, the nucleon resonance data, at $x \approx 0.1$, do not exhibit such a drastic collapse with Q^2 , and stay fairly constant. In fact, they still seem to oscillate around one Q^2 -independent global curve [13], informing us that the Q^2 dependence of the larger x nucleon resonance data is rather shallow. It is this behavior that makes the scaling curve in Eqn. 1, defined by the world's nucleon resonance F_2 data, look "valence-like" [13].

We emphasize here the difference in reaching the low Q^2 region for the various values of x (see also Fig. 4). For the DESY experiments, low Q^2 is established at small x by having a large (\approx constant) amount of energy transfer ν . For this reason, we naively expect this region to exhibit similar characteristics as the parton model. For the JLab/SLAC experiments at $x \approx 0.1$, one reaches low Q^2 at relatively small energy transfers. In fact, if one would restrict oneself to the nucleon resonance region ($M^2 < W^2 \leq 4$ GeV²), the nucleon resonances "slide" down the x scale to lower x for lower Q^2 (e.g., see the constant $W = 2$ GeV arrow in Fig. 4), where their strength dies out, as a function of Q^2 , due to gauge invariance.

III. MOMENTS OF F_2^P

Now, we construct both the Cornwall-Norton and Nachtmann moments from the world's data for the F_2 ($= \nu W_2$) structure function, for the Q^2 range up to 10 (GeV/c)². The Cornwall-Norton moments are defined as

$$M_n(Q^2) = \int_0^{x_{thr}} dx x^{n-2} \nu W_2(x, Q^2), \quad (2)$$

and the Nachtmann moments as

$$M_n(Q^2) = \int_0^{x_{thr}} dx \frac{\xi^{n+1}}{x^3} \left[\frac{3 + 3(n+1)r + n(n+2)r^2}{(n+2)(n+3)} \right] \nu W_2(x, Q^2). \quad (3)$$

Here, $r = (1 + 4M^2x^2/Q^2)^{1/2}$, and x_{thr} is Bjorken x for pion threshold. We add to these integrals the elastic contribution, at $x = 1$, where

$$\nu W_2(x, Q^2) = \delta(1-x) \frac{\left(G_E^2(Q^2) + \frac{Q^2}{4M^2} G_M^2(Q^2) \right)}{\left(1 + \frac{Q^2}{4M^2} \right)}. \quad (4)$$

G_E (G_M) is the proton electric (magnetic) form factor. For the proton form factors, we use a fit to the world's data by Bosted [31].

To obtain the inelastic contributions we integrate data like those shown in Figs. 1 and 3. Apart from the data shown in Fig. 1, we have added Q^2 points where additional data was available. For $Q^2 < 0.6$ (GeV/c)² we have constrained our search to elastic and nucleon resonance data. For $0.6 < Q^2 < 4$ (GeV/c)² we have used nucleon resonance data in combination with deep inelastic data, whereas for $Q^2 > 4$ (GeV/c)² we have constructed the moments utilizing both deep inelastic and nucleon resonance models, similar as in Ref. [32]. For the smallest values of Q^2 (< 0.6 (GeV/c)²), we assume a constant value of F_2 below x for $W^2 = 4.0$ GeV², as no data exists. As one can see from Fig. 3, this may not be a bad approximation for $Q^2 < 0.6$ (GeV/c)², especially since the nucleon resonance region data extend down to $x \leq 0.1$, and the integration area below $x = 0.1$ is expected to be small only. To judge the uncertainty in this procedure, we have also integrated the $Q^2 \approx 0.2$ (GeV/c)² data starting at $W^2 = 9.0$ GeV² (rather than $W^2 = 4.0$ GeV²). This changes the second moment by less than 3%. Lastly, in some cases, we used a model to construct data at fixed Q^2 , rather than allowing for the small range of Q^2 in the data. This effect on the second moments was found to be small, $< 3\%$, and far smaller on the higher moments. Thus, we believe the total uncertainty in the moments we calculate to be less than 5%. We show the values for the second, fourth, sixth, and eighth Cornwall-Norton (top) and Nachtmann (bottom) moments of the proton, extracted from the world's data, including deep inelastic, nucleon resonance, and elastic data, as described above, in Fig. 5. Similarly, Tables I and II list the numerical values of the moments, with the elastic contribution to each separately given.

As expected, the elastic contribution dominates the moments at the lowest Q^2 . Note that the Cornwall-Norton moments will become unity, i.e. the proton charge squared, at $Q^2 = 0$, whereas the Nachtmann moments will vanish at $Q^2 = 0$, as can readily be seen from Eqn. 3. We believe the latter is due to the fact that, with respect to Bjorken x , the Nachtmann scaling variable ξ correctly takes into account the finite proton mass scale [8], but does not account for any other significant mass scale (like the quark masses). As the interpretation of the Cornwall-Norton moments in the $Q^2 < 1$ (GeV/c)²

region seems more intuitive, and we are interested here in the low- Q^2 behavior of the moments, we will concentrate on these moments in the remainder of the discussions in this work. To emphasize that there is indeed not much difference between the Cornwall-Norton and Nachtmann moments if one concentrates on the low- Q^2 region where the elastic contribution turns dominant, Fig. 6 graphically displays the relative contribution of the elastic channel to the total moment for both Cornwall-Norton (top) and Nachtmann (bottom) moments, for $n = 2$ (solid circles), $n = 4$ (squares), $n = 6$ (triangles) and $n = 8$ (stars), from Tables I and II. Nonetheless, as the benefit of the Nachtmann moments is to push an analysis in terms of an Operator-Product Expansion to lower values of Q^2 , taking correctly target-mass effects into account, we show everywhere similar figures, for comparison, for the Nachtmann moments. Note that one can argue that the relative contribution of the elastic grows slower for $Q^2 \rightarrow 0$ if one uses the Nachtmann moments.

First, let us revisit the $Q^2 > 10$ (GeV/c) 2 behavior of the lower moments. For any non-singlet moment $M_n^{NS}(Q^2)$ QCD predicts [7,9] at asymptotically large Q^2 that

$$M_n^{NS}(Q^2) = A_n (\ln(Q^2/\Lambda^2))^{-1/d_n^{NS}}, \quad (5)$$

where Λ is the QCD scale parameter and

$$d_n^{NS} = \gamma_{o,n}^{NS}/2\beta_o, \quad (6)$$

where $\beta_o = 11 - (2/3)N_f$, with N_f the number of flavors, and $\gamma_{o,n}^{NS}$ are the leading-order non-singlet anomalous dimensions numerically specified in [7]. To circumvent the requirement of non-singlet moments we highlight in Fig. 7 the $n = 4$ moment: although we use the same F_2 structure function data for all moments, the weighting with x^{n-2} in these moments will emphasize the large- x region, at higher n , and thus approximate a non-singlet moment. On the top of Fig. 7 we show the Cornwall-Norton moment, on the bottom the Nachtmann moment (each to the power $-1/d_n^{NS}$). We show the data in a log-log plot, thus emphasizing the low- Q^2 region. The moments are shown both with (stars) and without (open circles) the elastic contribution included. The dashed curves exhibit a fit to the data, from [32], limited to $Q^2 > 20$ (GeV/c) 2 to minimize the effect of higher twist, in the form $P_1 \ln(Q^2/\Lambda^2)$. In [32], this fit gives $P_1 = 27.46$ (27.05 ± 0.25 (0.24)) and $\Lambda = 250$ MeV, for the Cornwall-Norton (Nachtmann) moment, rendering the expected logarithmic scaling behavior in QCD at asymptotic Q^2 . The dotted (dot-dashed) curves exhibit similar fits in the form $(P_1 + P_2/Q^2 + P_3/Q^4) \ln(Q^2/\Lambda^2)$ down to $Q^2 = 2.0$ (GeV/c) 2 from the same Reference [32], taking into account higher twist coefficients in terms of $1/Q^2$ and $1/Q^4$. Numerical values for the $1/Q^2$ and $1/Q^4$ coefficients are $P_2 = 0.33 \pm 0.04$ (0.33 ± 0.04) and $P_3 = 4.69 \pm 0.19$ (1.61 ± 0.15) for the Cornwall-Norton (Nachtmann) moment

(see also the caption of Fig. 7). One can easily verify from Fig. 7 that the magnitude of the P_3 coefficient is in this case dominated by the inclusion of the elastic contribution. Similarly, the Nachtmann ($n = 4$) moment analysis gives a drastically different value for P_3 from the Cornwall-Norton ($n = 4$) moment analysis mainly due to the different contribution by the elastic.

In Fig. 8 we show the second (Fig. 8a), fourth (8b), sixth (8c) and eighth (8d) Cornwall-Norton moments for $Q^2 < 5$ (GeV/c) 2 , separated in the elastic contribution (squares, due to our choice of vertical scale sometimes only visible at the higher Q^2), the contribution of the $N - \Delta$ transition region (triangles, $1.2 < W^2 < 1.9$ GeV 2), of the second resonance region (open circles, $1.9 < W^2 < 2.5$ GeV 2) and of the “deep inelastic” region (stars, $W^2 > 4$ GeV 2). The total moment is given by the solid circles, and the curves connect the various data to guide the eye. The chosen finite W^2 regions will start contributing to the moments at low Q^2 , recovering part of the loss of strength due to the fall-off of the elastic contribution, and then also die off, as the resonances move to the larger ξ side of the scaling curve. The contribution of the $W^2 > 4$ GeV 2 region does not die off, as this is not a finite W^2 region, so higher- W^2 resonances and/or higher- W^2 inelastic background start becoming important with increasing Q^2 , eventually yielding the logarithmic behavior of the moments prescribed by QCD. As evidenced by the difference between the $W^2 > 4$ (GeV) 2 contribution and the total moment, the contribution of the region of $W^2 < 4$ GeV 2 is non-negligible up to $Q^2 \approx 5$ (GeV/c) 2 , even for the second moment. Similar conclusions can be drawn from the various Nachtmann moments, shown in Fig. 9.

Although the dynamical origin of local duality is still not understood, it seems intricately intertwined with the behavior between the $Q^2 \rightarrow 0$ point, where only elastic scattering contributes to the moments, and $Q^2 > 5$ (GeV/c) 2 , where deep inelastic scattering already dominates the lower moments. In the region $0.2 < Q^2 < 5$ (GeV/c) 2 the nucleon resonances contribute to a substantial part of the moments, and, in their average, seem indistinguishable from deep inelastic scattering at $Q^2 > 1$ (GeV/c) 2 , consistent with the findings of Bloom and Gilman [1,2] and as quantitatively shown in Ref. [14] for the second moment. In the very low Q^2 transition region, $Q^2 < 1$ (GeV/c) 2 , the contribution of the coherent elastic peak to the second moment dies out, whereas the nucleon resonances already show the onset of their duality behavior, in that they tend to oscillate, already at $Q^2 \approx 0.2$ (GeV/c) 2 , around a smooth curve [13]. Furthermore, the nucleon resonances shuffle their strength around such that, at $Q^2 \approx 1$ (GeV/c) 2 , they have reached the same behavior as a function of x as one would expect from deep inelastic data.

We note here also that the behavior of the second Cornwall-Norton F_2 moment we extract is very similar to

the behavior in the second moment of the spin-dependent g_1 structure function [33]. Presently we only have sparse g_1 data in the nucleon resonance region, for $0.1 < Q^2 < 5$ $(\text{GeV}/c)^2$, such that we can not verify precisely whether the spin-dependent nucleon resonance data tend to oscillate around a similar smooth curve. However, the limited data are not inconsistent with such a behavior [34]. Also, we presently do not have enough data for the longitudinal structure function F_L to verify a similar onset of duality [35], although sparse hints do exist in the present world's data [36].

IV. DISCUSSION OF RESULTS

Our findings, that the moments of F_2 show a smooth transition from deep inelastic scattering down to $Q^2 \approx 0$ $(\text{GeV}/c)^2$, and that the nucleon resonances tend to oscillate around one smooth curve, support the findings of Ref. [37,38] that higher-twist effects are small if one looks at the low- Q^2 behavior of F_2 for $Q^2 \simeq 1$ $(\text{GeV}/c)^2$. The dynamical process of local duality dictates minimal Q^2 dependence of F_2 at small Q^2 ; in terms of the Operator-Product Expansion, this can be explained if the higher-twist effects are reduced *on average* in the nucleon resonance region [39]. Nonetheless, higher-twist effects must be responsible for the nucleon resonances themselves. The results for the lower moments of F_2 , presented here, show a forced transition from the elastic point to the large Q^2 limit, supported by the oscillations of the nucleon resonance region around one smooth curve at low Q^2 . This smooth curve resembles the deep inelastic data at $Q^2 \simeq 1$ $(\text{GeV}/c)^2$, and higher-twist effects continue to be small from there on.

The extension of a pQCD analysis to very low values of Q^2 (< 2 $(\text{GeV}/c)^2$) is hampered by the fact that here even the low n moments are mainly sensitive to the inclusion of the elastic contribution (as this contributes already close to 10% to the $n = 2$ moment at $Q^2 = 2$ $(\text{GeV}/c)^2$), thus soon rendering a meaningless interpretation in terms of higher-twist effects. If one would like to fit the moments to lower values of Q^2 , one would soon end up with coefficients for higher-twist coefficients (in an expansion of $(1/Q^2)^n$) that start being large, while subsequent coefficients will tend to opposite signs to cause the cancellation required to make the moment a slowly varying function of Q^2 only. These cancellations are evidently of non-perturbative origin and their origin has to be sought through mechanisms other than the twist expansion. Similarly, if one neglects the elastic channel, one will at low Q^2 be mainly sensitive to the imposed constraint by gauge invariance that the structure function F_2 must behave like $Q^2 \sigma(\gamma p)/(4\pi^2 \alpha_{em})$ [30].

At the values of x where the nucleon resonances are visible at low Q^2 in Fig. 3 (e.g. $x \approx 0.1$), the F_2 structure function does not yet linearly vanish with Q^2 yet,

as shown in [13]. Thus, although the F_2 strength in the nucleon resonance region has to disappear linearly with Q^2 below some Q_0^2 , one can argue that the behavior of the data is not reflecting this $Q^2 < Q_0^2$ expectation yet. This indicates that the oscillations the nucleon resonances exhibit around a smooth curve, even down to $Q^2 \approx 0.1$ $(\text{GeV}/c)^2$, is non-trivial. As the low- Q^2 F_2 data below $W^2 = 4$ GeV^2 predominantly consists of excited nucleon resonances, and hardly contributions from inelastic non-resonant processes, one can argue that such a smooth curve must be close to a curve consisting of valence strength only. In fact, the Q^2 dependence of the integrated valence quark strength in the GRV model [28,29] is close to the Q^2 dependence of the second Cornwall-Norton moment of F_2 . However, this Q^2 dependence is predominantly due to the inclusion of the elastic channel. Thus, for a picture such as the GRV model to be valid, there must be a separate Q^2 dependence for the vanishing of the large- x strength at small Q^2 (governed by the nucleon resonances) and the growth of the small- x sea.

V. CONCLUSIONS

We show that the world's data on F_2 , down to $Q^2 \simeq 1$ $(\text{GeV}/c)^2$, are reasonably well described by the GRV model. This includes the nucleon resonance data, which average to a scaling curve, due to local duality. Down to $Q^2 \simeq 0.1$ $(\text{GeV}/c)^2$, the nucleon resonance data still tend to oscillate around one smooth curve. The contribution of the nucleon resonances to the lower moments of F_2 die out at very small Q^2 as they have moved to smaller Bjorken x . Instead, the moments below $Q^2 \approx 1$ $(\text{GeV}/c)^2$ are governed by the elastic contribution. Thus, an analysis of the moments of F_2 in terms of the Operator-Product Expansion will render higher-twist terms which are predominantly due to the elastic contribution. Local duality seems to prescribe the transition from this elastic contribution to the logarithmic scaling region.

This work is supported in part by research grants from the U.S. Department of Energy and the National Science Foundation under Grant No. HRD-9633750 (Hampton). The authors express gratitude to the Jefferson Lab Theory Group for many useful discussions. CEK acknowledges the support of an NSF Early Faculty Career Development Award.

[1] E.D. Bloom and F.J. Gilman, Phys. Rev. D 4 (1970) 2901
[2] E.D. Bloom and F.J. Gilman, Phys. Rev. Lett. 25 (1970)

- [3] P.D.B. Collins, *An Introduction to Regge Theory and High Energy Physics* (Cambridge University Press, Cambridge, 1977)
- [4] F.E. Close, *An Introduction to Quarks and Partons* (Academic Press, Great Britain, 1979).
- [5] R. Roberts, *The Structure of the Proton* (Cambridge University Press, Cambridge, 1990)
- [6] G. Altarelli, Phys. Rep. **81** (1982) 1
- [7] A.J. Buras, Rev. Mod. Phys. **52** (1980) 199
- [8] O. Nachtmann, Nucl. Phys. **B63** (1975) 237.
- [9] D.W. Duke and R.G. Roberts, Nucl. Phys. **B166** (1980) 243.
- [10] A. DeRujula, H. Georgi, and H.D. Politzer, Phys. Lett. **B64** (1976) 428.
- [11] A. DeRujula, H. Georgi, and H.D. Politzer, Annals Phys. **103** (1977) 315.
- [12] X. Ji and P. Unrau, Phys. Rev. D **52** (1995) 73.
- [13] I. Niculescu *et al.*, Evidence for Valence-Like Quark-Hadron Duality, to be published in Phys. Rev. Lett. (2000).
- [14] I. Niculescu *et al.*, Experimental Verification of Quark-Hadron Duality, to be published in Phys. Rev. Lett. (2000).
- [15] S. Stein *et al.*, Phys. Rev. D **12** (1975) 1884.
- [16] C. Keppel, Proceedings of the Workshop on CEBAF at Higher Energies, Eds. N. Isgur and P. Stoler (1994) 237
- [17] J.M. Conrad, M.H. Shaevitz, and T. Bolton, Rev. Mod. Phys. **70** (1998) 1341.
- [18] P. Stoler, Phys. Rep. **226** (1993) 103.
- [19] L.W. Whitlow *et al.*, Phys. Lett. **B250** (1990) 193; L.W. Whitlow, Ph.D. Thesis, American University (1990); L. Tao *et al.*, Z. Phys. **C70**, 387 (1996);
- [20] M. Arneodo *et al.*, Nucl. Phys. **B483** (1997) 3.
- [21] M.R. Adams *et al.*, Phys. Rev. D **54** (1996) 3006.
- [22] S. Aid *et al.*, Nucl. Phys. **B470** (1996) 3.
- [23] M. Derrick *et al.*, Z. Phys. **C65** (1995) 379; *ibid.* **C69** (1995) 607.
- [24] M. Derrick *et al.*, Z. Phys. **C72** (1996) 399.
- [25] J. Breitweg *et al.*, Phys. Lett. **B407** (1997) 432.
- [26] J. Breitweg *et al.*, hep-ex/9809005 (1998).
- [27] J. Breitweg *et al.*, hep-ex/0005018 (2000).
- [28] M. Glück, E. Reya, and A. Vogt, Z. Phys. **C67** (1995) 433.
- [29] M. Glück, E. Reya, and A. Vogt, Eur. Phys. J. **C5** (1998) 461.
- [30] A. Donnachie and P.V. Landshoff, Z. Phys. **C61** (1994) 139.
- [31] P.E. Bosted, Phys. Rev. C **51** (1995) 409.
- [32] I. Niculescu, C. Keppel, S. Liuti, and G. Niculescu, Phys. Rev. D **60** (1999) 094001.
- [33] X. Ji and W. Melnitchouk, Phys. Rev. D **56** (1997) 1.
- [34] K. Abe *et al.*, Phys. Rev. D **58** (1998) 112003.
- [35] C. Carlson and N. Mukhopadhyay, Phys. Rev. D **41** (1990) 2343.
- [36] R. Ent, C.E. Keppel, and I. Niculescu, to be published in Phys. Rev. D (2000).
- [37] U.K. Yang and A. Bodek, Phys. Rev. Lett. **82** (1999) 2467.
- [38] S. Liuti *et al.*, to be published.
- [39] H. Georgi and H.D. Politzer, Phys. Rev. D **14** (1976) 1829.

TABLE I. Cornwall-Norton Moments for $n = 2, 4, 6,$ and 8 at $0.15 \leq Q^2 \leq 4.3$ (GeV/c)², as extracted from the data (see text). The elastic contribution is given as a separate column. The uncertainties of the total moments are smaller than 5%.

Q^2 (GeV/c) ²	elastic	$n = 2$	$n = 4$	$n = 6$	$n = 8$
0.15	0.592	0.652	0.594	0.592	0.592
0.20	0.504	0.584	0.508	0.505	0.504
0.45	0.249	0.379	0.261	0.251	0.250
0.55	0.195	0.341	0.210	0.198	0.196
0.85	0.103	0.278	0.122	0.107	0.104
0.94	0.087	0.264	0.107	0.092	0.088
1.40	0.040	0.231	0.064	0.047	0.043
1.70	0.026	0.219	0.051	0.034	0.029
2.40	0.011	0.203	0.036	0.019	0.014
3.00	0.006	0.196	0.030	0.013	0.009
3.30	0.005	0.192	0.028	0.012	0.008
4.30	0.002	0.184	0.023	0.008	0.005

TABLE II. Nachtmann Moments for $n = 2, 4, 6,$ and 8 at $0.15 \leq Q^2 \leq 4.3$ (GeV/c)², as extracted from the data (see text). The elastic contributions, different for each n , are given as a separate entity in the columns. The uncertainties of the total moments are smaller than 5%, and the numbers quoted can be used to this precision.

Q^2	$n = 2$		$n = 4$		$n = 6$		$n = 8$	
	elas.	total	elas.	total	elas.	total	elas.	total
0.15	0.274	0.333	0.040	0.041	0.0051	0.0052	0.0006	0.0006
0.20	0.256	0.322	0.047	0.049	0.0074	0.0075	0.0011	0.0011
0.45	0.160	0.281	0.050	0.057	0.0139	0.0146	0.0037	0.0038
0.55	0.131	0.268	0.046	0.056	0.0146	0.0157	0.0045	0.0046
0.85	0.076	0.243	0.034	0.047	0.0137	0.0157	0.0054	0.0057
0.94	0.065	0.235	0.030	0.045	0.0130	0.0154	0.0054	0.0058
1.40	0.032	0.217	0.018	0.036	0.0093	0.0128	0.0047	0.0055
1.70	0.022	0.209	0.013	0.033	0.0073	0.0114	0.0040	0.0051
2.40	0.010	0.197	0.007	0.027	0.0041	0.0089	0.0026	0.0040
3.00	0.005	0.192	0.004	0.024	0.0026	0.0075	0.0018	0.0033
3.30	0.004	0.189	0.003	0.023	0.0021	0.0071	0.0015	0.0031
4.30	0.002	0.181	0.001	0.020	0.0011	0.0058	0.0008	0.0024

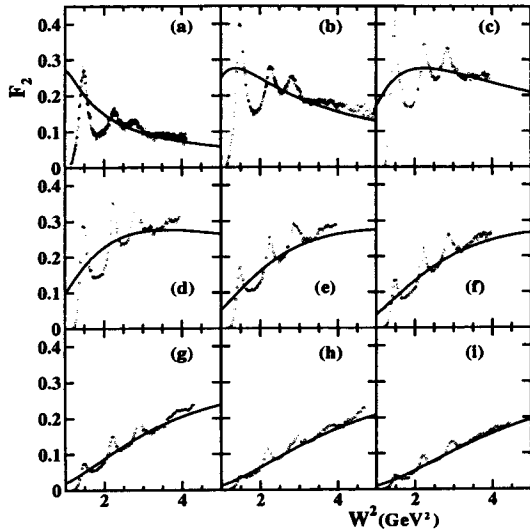


FIG. 1. F_2 Spectrum in the nucleon resonance region as a function of W^2 , for values of $Q^2 = 0.07$ (a), 0.20 (b), 0.45 (c), 0.85 (d), 1.40 (e), 1.70 (f), 2.40 (g), 3.00 (h) and 3.30 (i) $(\text{GeV}/c)^2$. We have superimposed the results from the scaling curve from Ref. [14], to illustrate the behavior of the nucleon resonance region with increasing Q^2 .

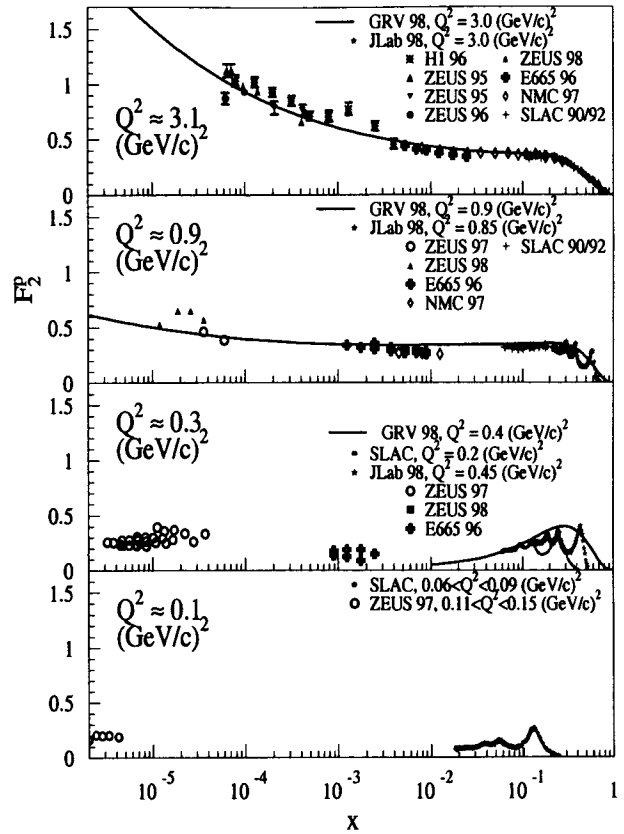


FIG. 3. F_2 as a function of x for four values of Q^2 , with a logarithmic x scale. The symbols indicate various experiments, as cited in the text. The solid curves in the top two panels represent the calculated distributions from the GRV collaboration [28,29], evolved from $Q^2 = 0.4$ $(\text{GeV}/c)^2$. The solid curve in the third panel represents the input distribution itself.

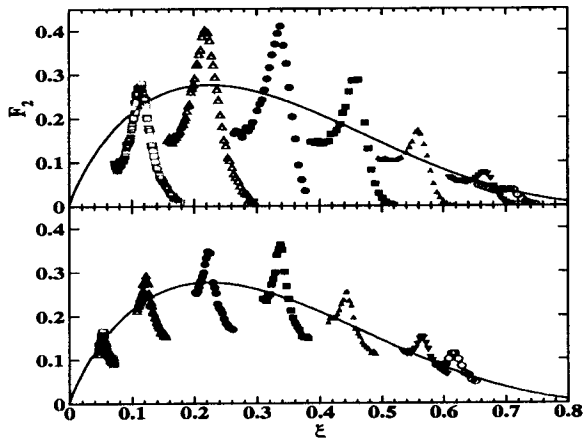


FIG. 2. F_2 data for the regions $1.2 < W^2 < 1.9$ (top) and $1.9 < W^2 < 2.5$ (bottom) GeV^2 , as a function of Nachtmann ξ . Data are shown for $Q^2 = 0.07, 0.20, 0.45, 0.85, 1.4, 2.4,$ and 3.0 $(\text{GeV}/c)^2$ (left to right), respectively. The solid curve represents the scaling curve, determined by averaging all nucleon resonance data [14].

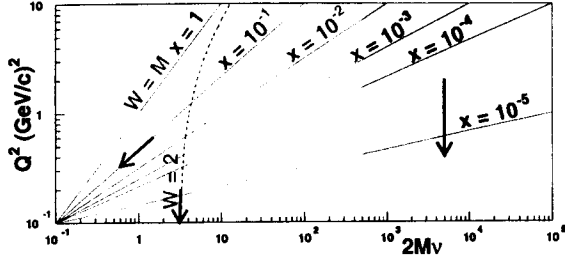


FIG. 4. Kinematics region of the world's F_2 structure function data, for $Q^2 < 10$ $(\text{GeV}/c)^2$. Thin lines are for fixed Bjorken x . The dashed line is for fixed $W = 2$ GeV, indicating the border of the region typically associated with the nucleon resonances (the other border being fixed $W = M$, or $x = 1$). The dashed area exhibits the kinematics region of the recent DESY measurements [22–26]. The thick arrows indicate various manners in which one can reach the limit $Q^2 \rightarrow 0$, at fixed x , fixed W , or fixed ν .

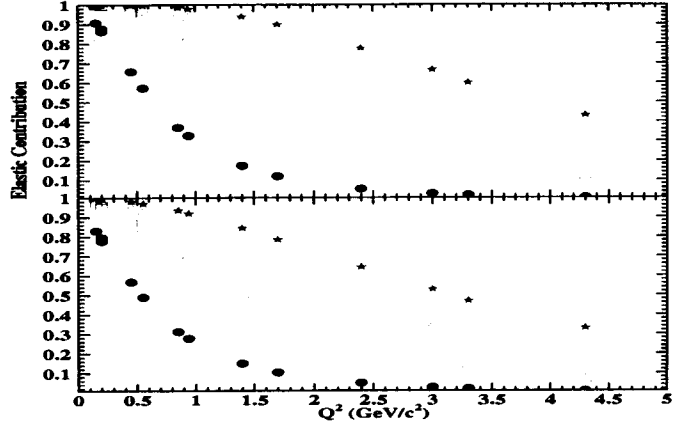


FIG. 6. Contribution of the elastic channel to the Cornwall-Norton moments (top) and Nachtmann moments (bottom) extracted from the world's electron-proton scattering data, for $n = 2$ (solid circles), 4 (squares), 6 (triangles), and 8 (stars), up to $Q^2 = 5$ $(\text{GeV}/c)^2$. The data are from Tables I and II.

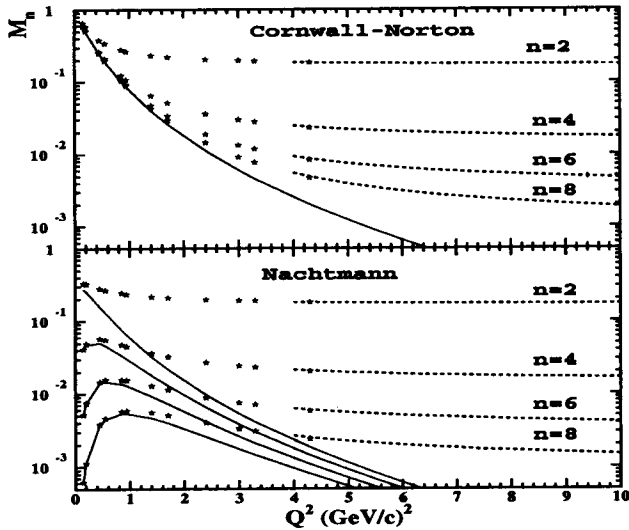


FIG. 5. Cornwall-Norton moments (top) and Nachtmann moments (bottom) extracted from the world's electron-proton scattering data, for $n = 2, 4, 6$, and 8. The solid curves indicate the elastic contribution. At low Q^2 (≤ 4.3 $(\text{GeV}/c)^2$) the moments (stars) are directly constructed from the world's electron-proton F_2 database (see text). At larger Q^2 , the moments have been extracted from appropriate fits to the world's data on inclusive scattering to both the nucleon resonance and deep inelastic regions [32].

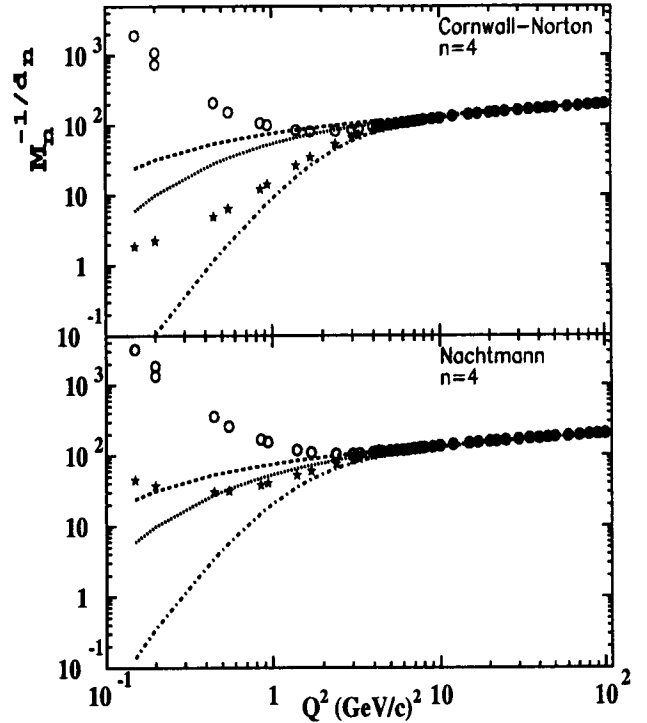


FIG. 7. Log-log plot of the $n = 4$ Cornwall-Norton (top) and Nachtmann (bottom) $M_n(Q^2)^{-1/d_n}$ moment as a function of Q^2 , where $d_n = \gamma_0^n/2\beta_0$ [5]. Stars (open circles) do (do not) include the elastic contribution. In the top plot, the dashed curve is a fit to the $n = 4$ moment in the form $P_1 \ln(Q^2/\Lambda^2)$, from [32], with $P_1 = 27.46 (\pm 0.25)$, and $\Lambda = 250$ MeV. Similarly, the dotted curve uses a form $(P_1 + P_2/Q^2) \ln(Q^2/\Lambda^2)$, with $P_2 = 0.33 (\pm 0.04)$, and the dot-dashed curve uses a form $(P_1 + P_2/Q^2 + P_3/Q^4) \ln(Q^2/\Lambda^2)$, with $P_3 = 4.69 (\pm 0.19)$. In the bottom plot, the fit parameters are $P_1 = 27.05 (\pm 0.24)$, $P_2 = 0.33 (\pm 0.04)$, and $P_3 = 1.61 (\pm 0.15)$, respectively [32].

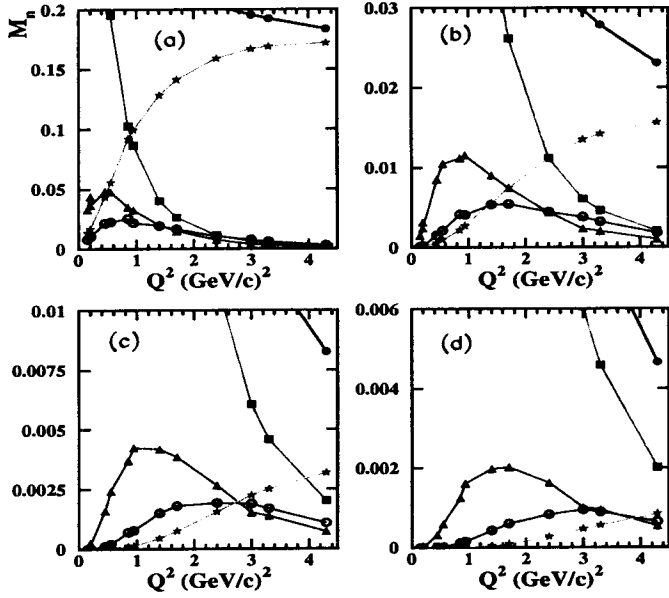


FIG. 8. Second (a), fourth (b), sixth (c) and eighth (d) Cornwall-Norton moments. Contributions due to the elastic peak (squares), the regions $1.2 < W^2 < 1.9$ GeV² (triangles), $1.9 < W^2 < 2.5$ GeV² (open circles), and $W^2 > 4$ GeV² (stars) are separately shown, in combination with the total moment (solid circles), as a function of the momentum transfer. Curves connect the various data, and are to guide the eye only.

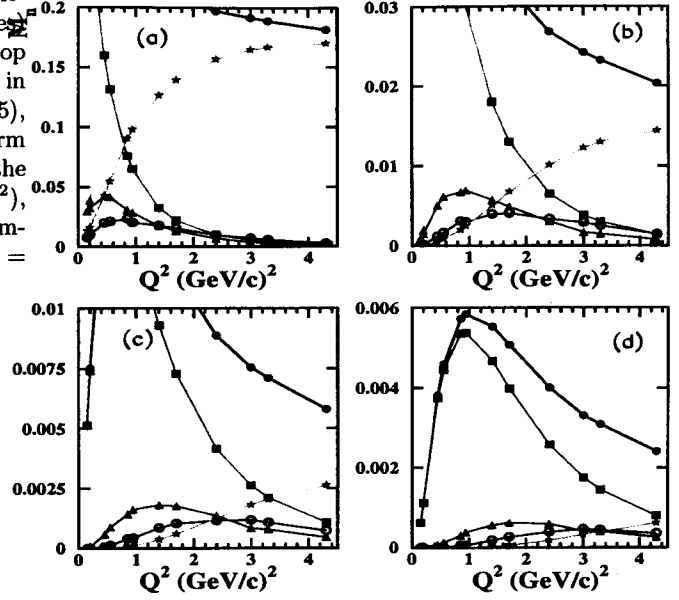


FIG. 9. Second (a), fourth (b), sixth (c) and eighth (d) Nachtmann moments. Contributions due to the elastic peak (squares), the regions $1.2 < W^2 < 1.9$ GeV² (triangles), $1.9 < W^2 < 2.5$ GeV² (open circles), and $W^2 > 4$ GeV² (stars) are separately shown, in combination with the total moment (solid circles), as a function of the momentum transfer. Curves connect the various data, and are to guide the eye only.